



**HAL**  
open science

# Procedure to construct three-dimensional models of geothermal areas using seismic noise cross-correlations: application to the Soultz-sous-Forêts enhanced geothermal site

Marco Calo', Xavier Kinnaert, Catherine Dorbath

## ► To cite this version:

Marco Calo', Xavier Kinnaert, Catherine Dorbath. Procedure to construct three-dimensional models of geothermal areas using seismic noise cross-correlations: application to the Soultz-sous-Forêts enhanced geothermal site. *Geophysical Journal International*, 2013, pp.doi: 10.1093/gji/ggt205. 10.1093/gji/ggt205 . hal-00840108

**HAL Id: hal-00840108**

**<https://hal.science/hal-00840108>**

Submitted on 18 Jun 2021

**HAL** is a multi-disciplinary open access archive for the deposit and dissemination of scientific research documents, whether they are published or not. The documents may come from teaching and research institutions in France or abroad, or from public or private research centers.

L'archive ouverte pluridisciplinaire **HAL**, est destinée au dépôt et à la diffusion de documents scientifiques de niveau recherche, publiés ou non, émanant des établissements d'enseignement et de recherche français ou étrangers, des laboratoires publics ou privés.

# Procedure to construct three-dimensional models of geothermal areas using seismic noise cross-correlations: application to the Soultz-sous-Forêts enhanced geothermal site

Marco Calò,<sup>1</sup> Xavier Kinnaert<sup>1,3</sup> and Catherine Dorbath<sup>1,2</sup>

<sup>1</sup>*EOST Institute, 5 rue René Descartes, 67084 Strasbourg cedex, France. E-mail: calo@unistra.fr*

<sup>2</sup>*IRD-UR234 (GET), Toulouse, France*

<sup>3</sup>*KIT Institute of Applied Geosciences, Geothermal Research, Adenauerring 20b, 76131 Karlsruhe, Germany*

Accepted 2013 May 16. Received 2013 May 15; in original form 2013 February 22

## SUMMARY

The aim of this work is to assess the feasibility of the noise-cross correlation tomography method for imaging and detecting potential geothermal reservoirs even in highly urbanised areas. We tested the noise correlation method to reconstruct the shape of the Soultz-sous-Forêts enhanced geothermal system (northern Alsace, France). We inverted Rayleigh waves (RWs) reconstructed from cross-correlations of 15 months of ambient seismic noise recorded by a seismic array installed around the Soultz geothermal power plant. By correlating noise records between 22 receivers, we reconstructed RWs with sufficient signal-to-noise ratio for 231 interstation paths. The reconstructed waveforms were used to estimate group velocity dispersion curves at periods between 1.0 and 5.0 s. The results were inverted for 2-D group velocity maps, and finally for a 3-D *S*-wave velocity model from 0 to 5.2 km depth. Our results clearly show the presence of low velocity bodies in the crystalline basement below the Soultz power plant at depth of 4–5 km, and at shallower depth (2.5–3.5 km) beneath the Rittershoffen and Woerth villages. These observations, in agreement with some previous studies, confirm that our procedure is suitable for geothermal exploration. Furthermore, the model presented here provides some suggestions to improve the existing geothermal power plant and inferences for further explorations in the area.

**Key words:** Interferometry; Hydrothermal systems; Seismic tomography; Crustal structure.

## INTRODUCTION

The Rhine Valley runs along the rift structure between Basel and Frankfurt with an average width of 35 to 40 km and a length of around 300 km (Fig. 1a) and offers particularly favourable conditions for geothermal energy development. The opening of the rift was achieved through a massive fracturing of the upper crust (Brun *et al.* 1991) characterized by large-scale normal faults striking more or less parallel to the Rhine Graben axis. A sedimentary cover, comprising mainly sandy marls with oil-bearing sand channels, overlies the granitic basement. The several profiles carried out (Elsass *et al.* 1995) have provided a detailed description of the tectonic structures in the sedimentary cover and in the upper part of the basement down to a depth of 2–2.5 km.

Some passive seismic tomographies, using regional and teleseismic data (Lopez-Cardozo & Granet 2005), provided a general view of the deeper structures. Nevertheless, the resolution of these velocity models is estimated to be 10–50 km resulting inadequate for investigating structures suitable for geothermal exploration, which requires to define bodies 1–5 km large. Furthermore, although active seismic imaging can provide the requested resolution, it is often

difficult to reach the target depth for exploitation and the costs are often prohibitive for small and medium business companies.

In the last decades, several projects have been approved for the exploration and exploitation of intermediate and deep (2–5 km depth) geothermal resources (e.g. Soultz, Basel, Landau, Insheim). The site of Soultz-sous-Forêts is the oldest one, and the most important from the scientific point of view. Several studies based on geophysical, geological and geochemical methods allowed describing the main features of this geothermal reservoir (e.g. Sanjuan *et al.* 2006; Dezayes *et al.* 2008; Dorbath *et al.* 2009 and references therein). Right now, the geothermal power plant of Soultz-sous-Forêts consists of three boreholes (GPK2, GPK3, GPK4) reaching a depth of about 5 km and one well (GPK1) drilled down to a depth of 3870 m. All the wells were stimulated throughout hydraulic injections in order to connect efficiently the boreholes to the fracture network and to improve the global permeability of the reservoir. Transient variations of the elastic parameters of the reservoir were observed applying 4-D seismic tomography techniques during some stimulations tests (Charl ty *et al.* 2006; Cuenot *et al.* 2008; Cal  *et al.* 2011; Cal  & Dorbath 2013). However, it was possible to apply the tomographic method only during the injection periods, i.e. when an

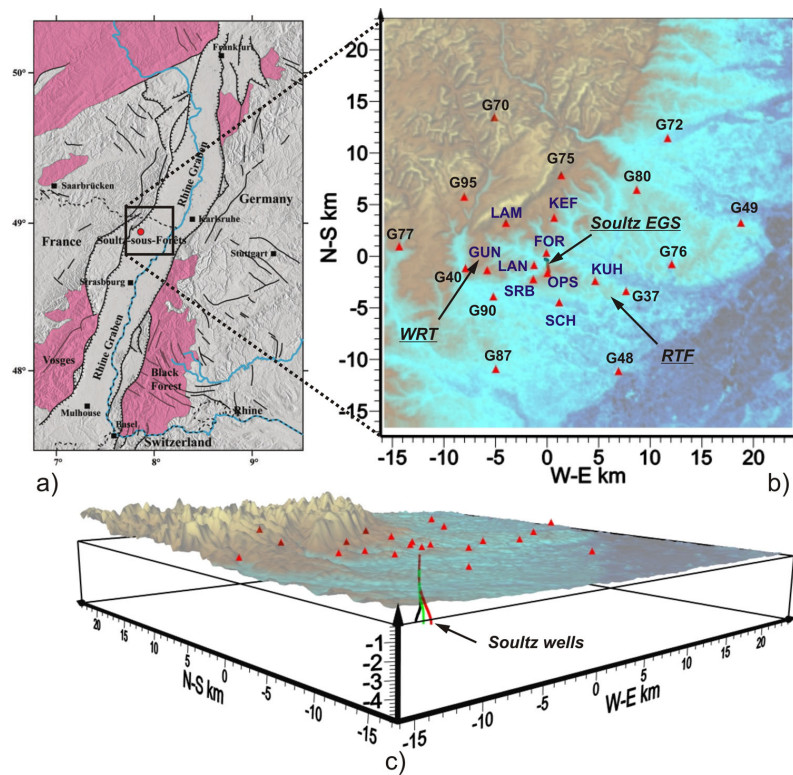


**Figure 1.** (a) Location of the Soutz-sous-Forêt in the Rhine Graben. Outcropping crystalline rock is in pink (from Dorbath *et al.* 2009). Black square is the target area; (b) permanent (blue) and temporary (black) stations used in this work. In the map are reported also the position of the Woerth (WRT) and Rittershoffen (RTF) towns; (c) 3-D view of the study area with the position of the seismic stations and of the wells of the Soutz EGS.

intense induced seismicity was recorded. Unfortunately, no information is available during the periods of rest because of the lack of an intense natural seismicity.

Recently, regional-scale noise cross-correlation tomography resulted as a powerful method to image crustal and upper-mantle seismic velocity structure without using ‘natural’ or ‘human’ seismic sources (Shapiro & Campillo 2004; Sabra *et al.* 2005; Shapiro *et al.* 2005; Campillo 2006). Since then, considerable researches on ambient noise tomography have been reported (e.g. Villaseñor *et al.* 2007; Yang *et al.* 2007; Bensen *et al.* 2008; Saygin & Kennett 2010; Stankiewicz *et al.* 2010; Li *et al.* 2012). Brenguier *et al.* (2007) showed for the first time the possibility to apply this technique at small scale by imaging the 3-D structures of the volcano Piton de la Fournaise. Recent studies have shown the possibility to retrieve signals from the noise cross-correlation at higher frequency ranges (1–30 Hz) and for different phases (e.g. the *P* waves; Roux *et al.* 2005) extending the reliability of the method also to image shallow structures of a few dozen of meters (Gouédard *et al.* 2012; Mordret *et al.* 2013).

In this work, we test the ability of the noise cross-correlation tomography method to image 3-D structures at small scale (about  $1 \times 1 \text{ km}^2$ ), and we propose the guidelines to apply it in regions characterized by high geothermal potential, and densely anthropized, as is the case of the upper Rhine valley.

## DATA PROCESSING

The seismic network used in this work is composed of 22 short period seismometers (Mark Products L4C 1 Hz). We used a homogeneous network in order to avoid the instrumental corrections. Nine stations are permanent sensors installed for the monitoring

of the Soutz-sous-Forêt enhanced geothermal system (EGS) site (Fig. 1b, in blue), while 13 sensors were installed in the framework of the European project GEISER from March 2011 to May 2012 (Fig. 1b, in black). Some preliminary studies were performed using only the permanent stations highlighting the necessity to enlarge the interstation distance for retrieving signals able to image the seismic features at depth of the Soutz Geothermal reservoir. Therefore, the temporary array was installed for 15 months. The seismic noise at the range of the frequencies considered in this work is essentially due to the strong human activity existing in the region then subjected to high variability. We observed also a daily azimuthal variation on the direction of the noise sources. However, the heterogeneity of the sources and their variability makes the sources of noise almost homogeneously distributed when a whole day of noise record is used to calculate the cross-correlation functions. This study uses only the vertical component signals of the stations and the seismic data were continuously recorded and sampled at 150 Hz.

We tested two procedures for the reconstruction of the Green’s Functions (GF). The first procedure is similar to that described by Bensen *et al.* (2007) where the data are windowed in 1-d segments, then bandpass filtered between 0.1 and 10 Hz and decimated to 37.5 samples per second. Subsequently, spectral whitening and one-bit normalization is applied to the records. The cross-correlation functions are then computed between signals of all possible pairs of stations. Finally, the traces are stacked day per day over 15 months and the GF filtered at different dominant periods. An example of reconstructed Rayleigh wave (RW) at 1.5 s dominant period is shown in Fig. 2a. Since we observed a satisfactory symmetry of the traveltimes picked on the causal and anticausal part of the signals, the final RW reconstruction was obtained averaging the two parts of the cross-correlation functions. An example of the final RW

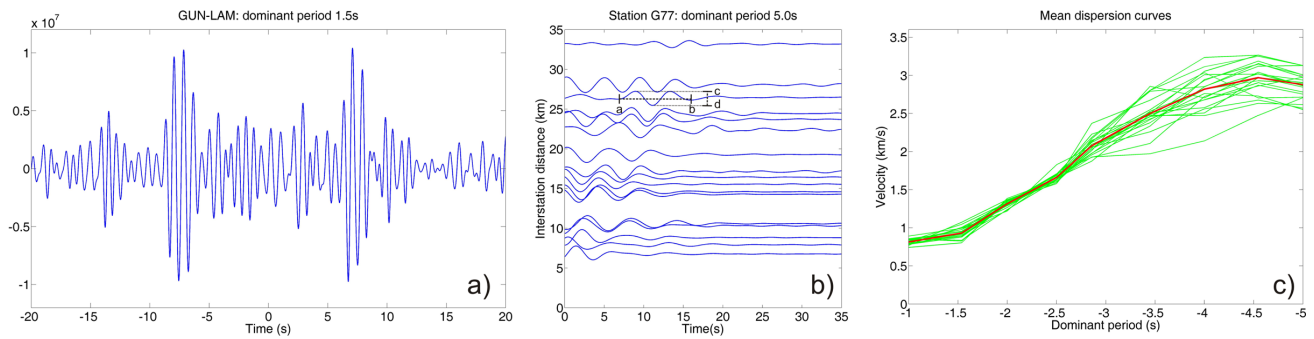


**Figure 2.** (a) Causal and anticausal reconstructed Rayleigh waves for a dominant period of 1.5 s; (b) folded cross-correlation functions between the station G77 and the rest of the network for the period of 5 s. a-b and c-d are the parameters used to calculate the factor form described in the text; (c) twenty-two average dispersion curves relative to the station used (green curves). The red curve is the average dispersion curve used as initial value for the tomographic inversions.

reconstructed between the station G77 and the rest of the network for the period of 5 s is reported in Fig. 2b. The second approach consisted on a preliminary filtering of the records using a narrow passband window centred on a dominant period followed by the spectral whitening, one-bit normalization and stacking of the cross correlated signals. Since the signals filtered at the same period obtained by the two procedures resulted equivalent, we selected the first one because less time consuming.

Therefore, we estimated a group velocity dispersion curve for each trace using a semi-automatic traveltimes picking procedure. The traveltimes were estimated as the maximum of the envelope of the time derivative of the noise cross-correlation (Shapiro & Campillo 2004; Sabra *et al.* 2005). The envelope is computed by using the Hilbert transform.

For each considered period, the semi-automatic procedure is based on a preliminary manual picking of the clearest GF retrieved for some pair of stations in order to estimate an initial group velocity, and in a subsequent automatic research of the maxima for the other traces using the mean group velocity previously calculated. Then we selected only the traveltimes picked on the maxima of the GF that respect a factor form calculated on the clearest GF manually picked. The factor form is calculated for each dominant period considered and is computed using the time length (a-b in Fig. 2b) of the GF and the distance between the maximum and the minimum of the signal (c-d in Fig. 2b). We finally eliminated the traveltimes of stations that have interdistance less than two times the considered dominant period.

By using these traveltimes and the distance between the stations, the group velocity for each station pair is computed for nine dominant periods equal to 1, 1.5, 2, 2.5, 3, 3.5, 4, 4.5 and 5 s. Finally, we averaged the dispersion measurements for each station in order to obtain 22 dispersion curves (green in Fig. 2c) and we calculated an average reference dispersion curve of the region by averaging the 22 dispersion curves previously calculated (red in Fig. 2c). The average 1-D dispersion curve is used as initial velocity model to compute the 2-D dispersion maps.

## 2-D TOMOGRAPHIC INVERSION

We applied the 2-D tomographic inversion technique of Barmin *et al.* (2001) for estimating the group velocity variations derived from the dispersion measurements. This method treats the surface waves as rays that sample an infinitesimal zone along the great circle linking two stations (source and receiver) and the regularization is based on minimizing a penalty function composed of a linear combination of data misfit and model smoothness. We optimized

the damping and smoothing parameters performing a series of tests using different combinations of these parameters considering data misfit, model resolution and model norm and by constructing the empirical trade-off curves (Hansen 1992; Evans & Achauer 1993). Since the amount of ray paths used to calculate the dispersion maps ranges between 198 and 85 for the periods of 1 and 5 s, respectively, the damping of the resolution matrix was optimized for each considered period. The 2-D model consists of  $37 \times 27 = 999$  cells of size  $1 \times 1 \text{ km}^2$ . To be consistent with previous studies, we chose GPK1 wellhead (48.93537 N, 7.86535 E, altitude 153 m) as the geographical origin for the inversion grid.

In Fig. 3 are reported the distributions of RW group velocities as anomalies with respect to the reference velocity values at 1, 3 and 5 s. The dispersion maps at these periods most likely refer to the seismic velocity field in the sedimentary cover (1 s), in the upper part of the geothermal reservoir (3 s) and in the lower one (5 s). The separation in depth of the reservoir is marked by a petrographic facies variation (Genter *et al.* 2000) and by the fact that the lower reservoir is much more fractured due to the deep stimulation tests conducted between 2000 and 2005. However, the tomographic maps clearly show the changing of the velocity pattern with the increasing of the dominant period considered, suggesting the presence of seismic velocity heterogeneities both in the horizontal and vertical directions.

To assess the reliability of the velocity pattern imaged, we built a synthetic model characterized by a low cross-shaped velocity anomaly of  $-10$  per cent with respect to the initial 1-D velocity model (black line in Fig. 3). The cross is centred on the EGS Soultz site. With the same configuration of the stations as in the real inversion, we calculated synthetic traveltimes for the nine periods considered. The inversion of the synthetic data shows that the anomaly is well located and its shape is adequately reconstructed in the well-resolved area (Fig. 3). Considering the parts of the model recovered using the synthetic data, the well-resolved area was estimated of  $30 \times 15 \text{ km}^2$  in E-W and N-S directions, respectively. It is worth noting that the decreasing of the restoration with the increasing of the dominant period is related to the decreasing of the number of traveltimes available.

## DEPTH INVERSION AND 3-D S-VELOCITY MODEL CONSTRUCTION

To obtain a 3-D model, we computed the tomographic dispersion maps for the nine considered periods using the same cell configuration. For each cell, we constructed a dispersion curve and we fitted these curves by polynomial functions in a least-squares sense. In the

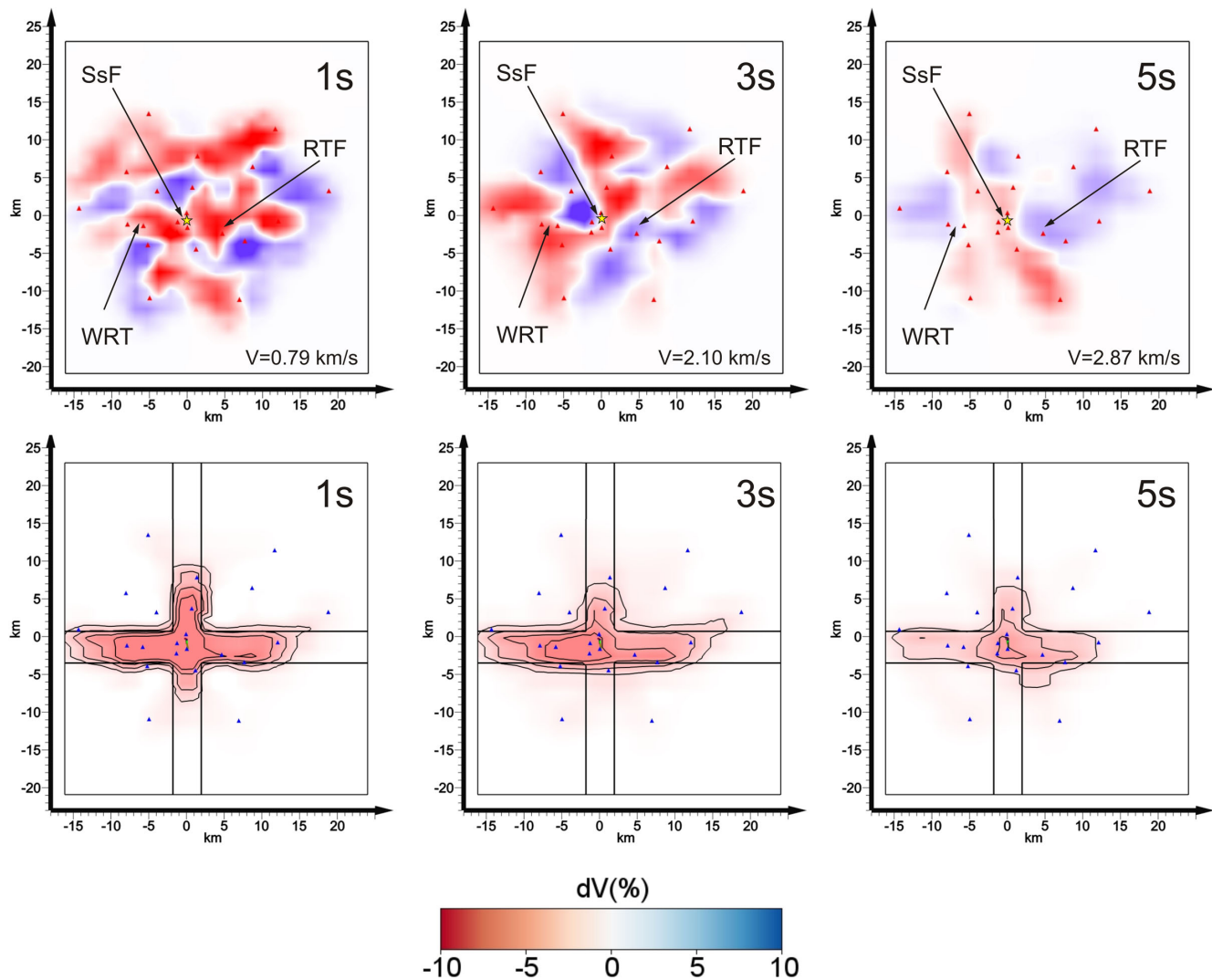


**Figure 3.** Top panels: Rayleigh group velocity map reported as anomaly with respect to the reference velocity values at 1, 3 and 5 s. Bottom panels: results of the test performed using synthetic traveltimes calculated in a model characterized by a low cross-shaped velocity anomaly of  $-10$  per cent with respect to the reference velocity for the periods of 1, 3 and 5 s. Black lines mark the shape of the cross-shaped true model.

inversion, only shear wave velocities are inverted.  $P$ -wave velocity and density are maintained fixed at values derived from geophysical logs performed in the Soutz-sous-Forêts boreholes (Beauce *et al.* 1991; Grecksch *et al.* 2003). The initial 1-D model has 13 layers, which are on average 0.4 km thick and match with the main change of the  $V_p$  model in depth. We thus obtained a  $V_s$  versus depth velocity profile for each cell by applying the method of Herrmann & Ammon (2002) that use an iterative damped least-square approach. We performed several tests using different configurations of the input parameters (e.g. damping, smoothing and number of iterations) to assess the stability of the results. In Fig. 4 is reported an example of the depth inversion result for one of the dispersion curves. The mean  $SD$  between the 999 observed and calculated dispersion curves is 0.35 s. Finally, the 1-D profiles are combined into 3-D shear wave velocity model. We spatially smoothed the 3-D velocity distribution in order to avoid sharp horizontal velocity gradients (Breguier *et al.* 2007).

In Fig. 4, we present two horizontal slices of the model, at 3 and 4.6 km, and two vertical sections (A–B and C–D), in the N–S and E–W directions. The model is represented as variations

in percentage with respect to the 1-D reference velocity model. Parts of the model poorly resolved are shadowed. The horizontal slice at 3 km shows the velocity pattern in the upper part of the crystalline basement. At this depth, the EGS site of Soutz does not seem to be characterized by particular velocity structures. Low seismic velocities are mostly located in the northern part, and in the southern and western part of the geothermal power plant. At greater depth, a 6–8 km low  $V_s$  body elongated in the N–S direction involves the deep geothermal reservoir. The deepest wells of the geothermal power plant (GPK2, GPK3, GPK4, Fig. 4 section AB) reach this low seismic anomaly while the shallower one (GPK1) stops at its top. In section C–D (Fig. 4), the low  $V_s$  anomaly is 2–4 km wide and mainly located west of the EGS boreholes. This section presents also two low velocity anomalies shallower than the one associated with the Soutz reservoir. A low  $V_s$  region (2.5–4 km deep) is located approximately beneath the village of Woerth and another one, less marked but much larger, located at a depth of 1.5–3.5 km, slightly at NE of the Rittershoffen village. High velocity regions separate the bodies at lower seismic velocity. Finally, both vertical sections report shallow seismic velocity anomalies

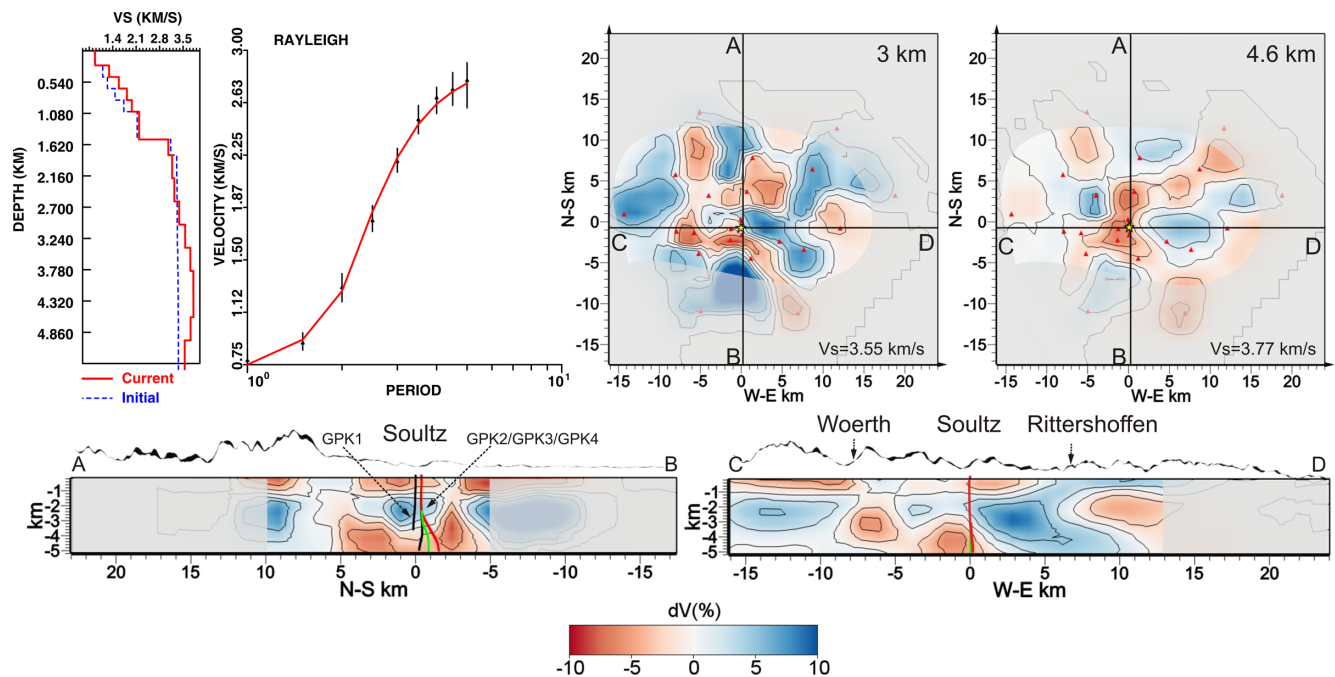


**Figure 4.** Top panels: example of the depth inversion of one cell dispersion model and horizontal slices at 3 and 4.6 km of the 3-D reconstructed model. Bottom panels; vertical sections (AB and CD), in the N–S and E–W directions of the 3-D model. The model is represented as variations in percentage with respect to the 1-D reference velocity model. Parts of the model not resolved are masked.

(0–1.6 km), which are related to the sedimentary layers of the Rhine Graben.

## DISCUSSION AND CONCLUSIONS

This study confirms the suitability of the seismic noise cross-correlation tomography for characterising geothermal reservoirs, also in densely populated regions such as is the case of the Rhine valley, where seismic noise sources are mostly originated by the human activity.

We used 15 months of seismic noise recorded by 22 stations deployed in the Soutz-sous-Forets region to retrieve RW between each pair of seismic sensors. Nevertheless, we tested that the emergence of the RW from cross-correlation with sufficient signal-to-noise ratio was observed after a stacking of only few days and therefore it is worth considering to perform a similar study using shorter temporal records. We used these waveforms to perform a RW tomography and invert dispersion curves extracted from nine group velocity maps in order to build a 3-D *S*-wave velocity model of the Soutz region. Synthetic tests allowed assessing the resolution and the reliability of the seismic velocity anomalies observed in the experimental velocity model.

We can relate the low velocity anomalies located in the crystalline basement to the presence of deep and intermediate geothermal reservoirs giving also inferences on their volumetric size.

Our results agree with other studies based on geochemical analyses and ground water circulation that suggest the presence of ‘hot-spot’ geothermal reservoirs in the crystalline basement of the Rhine Valley (Schellschmidt & Clauser 1996; Pribnow & Schellschmidt 2000; Clauser *et al.* 2002). The position of the anomalous body associated with the Soutz geothermal reservoir suggests that the actual boreholes intercept the main anomaly at its boundary. Nonetheless, we have to recall that the site of Soutz-sous-Forets has been object

of huge stimulations in the past and we cannot exclude that the low seismic velocity anomaly is the result of these injections. However, Schellschmidt & Clauser (1996), in a study of modelling of the thermal regime in the region, have already shown a similar pattern but at a depth of 800 m. This suggests that the velocity pattern observed in our model at greater depth is probably related to the seismic structure of the reservoir. This inference should be taken into account for future improvement of the power plant. The site of Rittershoffen is already known in the region and a project for the exploitation of intermediate-deep geothermal energy started in 2012. The lower amplitude of the anomaly imaged beneath Rittershoffen with respect to that of Soutz is in agreement with the thermal modelling proposed by Guillou-Frottier *et al.* (2012). Conversely, the velocity anomalies imaged beneath Woerth were not documented before and should be object of further investigations for geothermal exploitation in this area.

The procedure applied here should be considered as a guideline to follow for a reliable employment of this technique for the 3-D imaging of the geothermal reservoirs. Furthermore, cross-correlation of ambient noise should be also applied to develop geothermal monitoring systems. Duputel *et al.* (2009) and Brenguier *et al.* (2011) showed that in the volcano Piton de la Fournaise it was possible to detect very small velocity changes (0.1 per cent) with a time resolution as small as 1 d using noise cross-correlations analysis. These small variations were interpreted as the result of the change of the rock properties associated with dike intrusions and volcanic eruptions. Strong seismic velocity variations were already observed in the Soutz reservoir during injection tests (Calò *et al.* 2011; Calò & Dorbath 2013). These transient variations are interpreted as a result of sudden changes of the stress field due to large aseismic slips reaccommodating the stress perturbations. Adelinet *et al.* (2013) show that these variations may be related to changes of the aspect ratio of the fractures in agreement with variations of the *S*-wave anisotropy observed during the injections. However, temporal seismic velocity

variations should also occur during circulation tests. Often, induced seismicity is weak in these periods and making difficult a reliable assessment of the variation of the elastic parameters. Furthermore, small variations such as of 0.1 per cent will be difficult to observe with the traditional tomographic methods. Therefore, the use of the noise correlation method will result a useful tool for monitoring these possible changes of the elastic properties in order to understand the behaviour of a geothermal reservoir during the exploitation periods.

In conclusion, this preliminary study demonstrates that the noise cross-correlation tomography is a convenient technique for studying geothermal reservoirs. We were able to image the main features of the Soutlz EGS and we gave inferences for improving the exploitation of the geothermal reservoir. Some low seismic anomalies infer on the presence of new geothermal reservoirs although further investigations are necessary for a proper assessment on the exploitation possibilities.

Finally, the procedure that we have applied in this work can easily be implemented in other regions for geothermal explorations.

## ACKNOWLEDGEMENTS

This work was funded by the European project GEISER (FP7: 241321). We sincerely thank M. Campillo for the fruitful and constructive discussions. We thank Helene Jund and Hervé Wolding for the technical support and also we thank all the people who allowed the installation of the temporary network on their gardens. We thank the GEIE for the density borehole data.

## REFERENCES

- Adelinet, M., Dorbath, C., Calò, M., Dorbath, L. & Le Ravalec, M., 2013. Crack features and shear-wave splitting associated with dilatancy during hydraulic stimulation of the geothermal reservoir in Soultz-sous-Forêt, *Geophys. J. Int.*, in revision.
- Barmin, M., Ritzwoller, M. & Levshin, A., 2001. A fast and reliable method for surface wave tomography, *Pure appl. Geophys.*, **158**(8), 1351–1375.
- Beauce, A., Fabriol, H., Le Masne, D., Cavoit, C., Mechler, C. & Chen, X., 1991. Seismic studies on the HDR site of Soultz-sous-Forêts (Alsace, France), *Geotherm. Sci. Technol.*, **4**, 239–266.
- Bensen, G.D., Ritzwoller, M.H., Barmin, M.P., Levshin, A.L., Lin, F., Moschetti, M.P., Shapiro, N.M. & Yang, Y., 2007. Processing seismic ambient noise data to obtain reliable broad-band surface wave dispersion measurements, *Geophys. J. Int.*, **169**, 1239–1260.
- Bensen, G.D., Ritzwoller, M.H. & Shapiro, N.M., 2008. Broadband ambient noise surface wave tomography across the United States, *J. geophys. Res.*, **113**, doi:10.1029/2007JB005248.
- Brenguier, F., Shapiro, N.M., Campillo, M., Nercessian, A. & Ferrazzini, V., 2007. 3-D surface wave tomography of the Piton de la Fournaise volcano using seismic noise correlations, *Geophys. Res. Lett.*, **34**, L02305, doi:10.1029/2006GL028586.
- Brenguier, F., Clarke, D., Aoki, Y., Shapiro, N.M., Campillo, M. & Ferrazzini, V., 2011. Monitoring volcanoes using seismic noise correlations, *Comptes Rendus Géosc.*, **343**(8–9), 633–638.
- Brun, J.P. & Wenzel, F., 1991. Crustal scale structure of the southern Rhine Graben from ECORS-DEKORP seismic reflection data, *Geology*, **19**, 758–762.
- Calò, M., Dorbath, C., Cornet, F.H. & Cuenot, N. the ECORS-DEKORP Team, 2011. Large-scale aseismic motion identified through 4-D *P*-wave tomography, *Geophys. J. Int.*, **186**, 1295–1314.
- Calò, M. & Dorbath, C., 2013. Different behaviours of the seismic velocity field at Soultz-sous-Forêts revealed by 4D seismic tomography: case study of GPK3 and GPK2 injection tests, *Geophys. J. Int.*, doi:10.1093/gji/ggt153.
- Campillo, M., 2006. Phase and correlation in ‘random’ seismic fields and the reconstruction of the Green function, *Pure appl. Geophys.*, **163**, 475–502.
- Charl ty, J., Cuenot, N., Dorbath, C. & Dorbath, L., 2006. Tomographic study of the seismic velocity at the Soultz-sous-For ts EGS/HDR site, *Geothermics*, **35**, 532–543.
- Clauser, C., Griesshaber, E. & Neugebauer, H.J., 2002. Decoupled thermal and mantle helium anomalies: implications for the transport regime in continental rift zones, *J. Geophys. Res.*, **107**(B11), doi:10.1029/2001JB000675.
- Cuenot, N., Dorbath, C. & Dorbath, L., 2008. Analysis of the microseismicity induced by fluid injection in the Hot Dry Rock site of Soultz-sous-For ts (Alsace, France): implications for the characterization of the geothermal reservoir properties, *Pure appl. Geophys.*, **165**, 797–828.
- Dezayes, C., Genter, A., Thinon, I., Courrioux, G. & Tourli re, B., 2008. Geothermal potential assessment of Clastic triassic reservoirs (upper Rhine Graben, France), in *Proceeding of the Thirty-Second Workshop on Geothermal Reservoir Engineering Stanford University*, Stanford, California, January 28–30, 2008.
- Dorbath, L., Cuenot, N., Genter, A. & Frogneux, M., 2009. Seismic response of the fractured and faulted granite of Soultz-sous-For ts (France) to 5 km deep massive water injections, *Geophys. J. Int.*, **177**, 653–675.
- Duputel, Z., Ferrazzini, V., Brenguier, F., Shapiro, N.M., Campillo, M. & Nercessian, A., 2009. Real time monitoring of relative velocity changes using ambient seismic noise on the Piton de la Fournaise volcano (La Reunion) from January 2006 to June 2007, *J. Volc. Geotherm. Res.*, **184**, 164–173.
- Elsass, P., Aquilina, L., Beauce, A., Benderitter, Y., Fabriol, H., Genter, A. & Pauwels, H., 1995. Deep structures of the Soultz-sous-For ts HDR site (Alsace, France), in *Proceedings of the World Geothermal Congress*, Florence, Italy, pp. 2543–2647.
- Evans, J. & Achauer, U., 1993. Teleseismic velocity tomography using the ACH method: theory and application to continental-scale studies, in *Seismic Tomography: Theory and Practice*, pp. 319–360, Chapman & Hall, London.
- Genter, A., Traineau, H., Led sert, B., Bourguine, B. & Gentier, S., 2000. Over 10 years of geological investigations within the HDR Soultz project, France, in *Proceedings of the World Geothermal Congress 2000 Kyushu - Tohoku*, Japan, pp. 3707–3712.
- Gou dard, P., Yao, H., Ernst, F. & van der Hilst, R.D., 2012. Surface wave eikonal tomography in heterogeneous media using exploration data, *Geophys. J. Int.*, **191**, 781–788.
- Grecksch, G., Ortiz, A. & Schellschmidt, R., 2003. HDR project Soultz – thermophysical study of GPK2 and GPK3 granite samples. GGA Internal report, ENK5-CT-2000–00301.
- Guillou-Frottier, L., Carre, C., Bourguine, B., Bouchot, V. & Genter, A., 2012. Hydrothermal convection beneath an inclined basement-sediment interface: application to the Rhine Graben and its Soultz-sous-For ts temperature anomaly, in *Proceedings of the AGU Fall Meeting*, San Francisco, V13C-2856. 3–7 December.
- Hansen, P.C., 1992. Analysis of discrete ill-posed problems by means of the L-curve, *SIAM Rev.*, **34**, 561–580.
- Herrmann, R.B. & Ammon, C.J., 2002. Computer Programs in Seismology: Surface Waves, Receiver Functions and Crustal Structure, St. Louis Univ., St. Louis, MO.
- Li, H., Li, S., Song, X.D., Gong, M., Li, X. & Jia, J., 2012. Crustal and uppermost mantle velocity structure beneath northwestern China from seismic ambient noise tomography, *Geophys. J. Int.*, **188**, 131–143.
- Lopez-Cardozo, G. & Granet, M., 2005. A multi-scale approach to study the lithospheric structure of the southern Upper Rhine Graben; from seismic tomography through reflection seismics to surface geology, *Int. J. Earth Sci.*, **94**, 615–620.
- Mordret, A., Land s, M., Shapiro, N.M., Singh, S.C., Roux, P. & Barkved, O.I., 2013. Near-surface study at the Valhall oil field from ambient noise surface wave tomography, *Geophys. J. Int.*, **193**, 1627–1643.
- Pribnow, D. & Schellschmidt, R., 2000. Thermal tracking of upper crustal fluid flow in the Rhine Graben, *Geophys. Res. Lett.*, **27**(13), 1957–1960.

- Roux, P., Sabra, K.G., Gerstoft, P., Kuperman, W.A. & Fehler, M.C., 2005. P-waves from cross-correlation of seismic noise, *Geophys. Res. Lett.*, **32**, L19303, doi:10.1029/2005GL023803.
- Sabra, K.G., Gerstoft, P., Roux, P., Kuperman, W.A. & Fehler, M.C., 2005. Surface wave tomography from microseism in southern California, *Geophys. Res. Lett.*, **32**, L14311, doi:10.1029/2005GL023155.
- Saygin, E. & Kennett, B.L.N., 2010. Ambient seismic noise tomography of Australian continent, *Tectonophysics*, **481**, 116–125.
- Sanjuan, B. *et al.*, 2006. Tracer testing of the geothermal heat exchanger at Soultz-sous-Forêts (France) between 2000 and 2005, *Geothermics*, **35**(5–6), 622–653.
- Schellschmidt, R. & Clauser, C., 1996. The thermal regime of the Upper Rhine Graben and the anomaly of Soultz, *Z. Angew. Geol.*, **42**(1), 40–44.
- Shapiro, N.M., Campillo, M., Stehly, L. & Ritzwoller, M., 2005. High resolution surface-wave tomography from ambient seismic noise, *Science*, **307**, 1615–1618.
- Shapiro, N.M. & Campillo, M., 2004. Emergence of broadband Rayleigh waves from correlations of the ambient seismic noise, *Geophys. Res. Lett.*, **31**, L07614, doi:10.1029/2004GL019491.
- Stankiewicz, J., Ryberg, T., Haberland, C., Fauzi & Natawidjaja, D., 2010. Lake Toba volcano magma chamber imaged by ambient seismic noise tomography, *Geophys. Res. Lett.*, **37**, L17306, doi:10.1029/2010GL044211.
- Villaseñor, A., Yang, Y., Ritzwoller, M.H. & Gallart, J., 2007. Ambient noise surface wave tomography of the Iberian Peninsula: implications for shallow seismic structure, *Geophys. Res. Lett.*, **34**, L11304, doi:10.1029/2007GL030164.
- Yang, Y., Ritzwoller, M.H., Levshin, A.L. & Shapiro, N.M., 2007. Ambient noise Rayleigh wave tomography across Europe, *Geophys. J. Int.*, **168**, 259–274.

## SUPPORTING INFORMATION

Additional Supporting Information may be found in the online version of this article:

**Figure S1.** Upper part of the figure reports the diagonal elements of the covariance matrix calculated for the dispersion maps at 1, 3 and 5 s. Figures display that the central parts of the investigated area are enough resolved even for the period at 5 s. Lower part of the figure reports the empirical curves constructed for the empirical optimization of the damping for the dispersion maps at 1, 3, and 5 s. Each inversion was obtained with a different damping value. Arrows indicate the values of data variance and model length of the inversion selected (<http://gji.oxfordjournals.org/lookup/suppl/doi:10.1093/gji/ggt205/-/DC1>).

Please note: Oxford University Press are not responsible for the content or functionality of any supporting materials supplied by the authors. Any queries (other than missing material) should be directed to the corresponding author for the article.